Electrocardiology Modeling After Catheter Ablations for Atrial Fibrillation

Simone Nati Poltri, Guido Caluori, Pierre Jaïs, Annabelle Collin, Clair Poignard

▶ **To cite this version:**

Simone Nati Poltri, Guido Caluori, Pierre Jaïs, Annabelle Collin, Clair Poignard. Electrocardiology Modeling After Catheter Ablations for Atrial Fibrillation. FIMH 2023 - 12th International Conference Functional Imaging and Modeling of the Heart, Jun 2023, Lyon, France. pp.184-193, ⟨10.1007/978-3-031-35302-4_19⟩. ⟨hal-04155159⟩

HAL Id: hal-04155159

https://hal.science/hal-04155159v1

Submitted on 7 Jul 2023

HAL is a multi-disciplinary open access archive for the deposit and dissemination of scientific research documents, whether they are published or not. The documents may come from teaching and research institutions in France or abroad, or from public or private research centers.

L'archive ouverte pluridisciplinaire **HAL**, est destinée au dépôt et à la diffusion de documents scientifiques de niveau recherche, publiés ou non, émanant des établissements d'enseignement et de recherche français ou étrangers, des laboratoires publics ou privés.

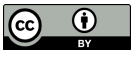

Distributed under a Creative Commons CC BY 4.0 - Attribution - International License

Electrocardiology Modeling after Catheter Ablations for Atrial Fibrillation

Simone Nati Poltri[1], Guido Caluori[2,3], Pierre Jaïs[2,3,4], Annabelle Collin[1], and Clair Poignard[1]

[1]Univ. Bordeaux, CNRS, INRIA, Bordeaux INP, IMB, UMR 5251, 33400 Talence, France; e-mail: {simone.nati-poltri, annabelle.collin}@inria.fr
[2]IHU LIRYC, Electrophysiology and Heart Modeling Institute, Fondation Bordeaux Université, 33600 Pessac, France
[3]Univ. Bordeaux, INSERM UMR 1045, CRCTB, 33600 Pessac, France
[4]CHU Bordeaux, Department of Electrophysiology and Cardiac Stimulation, 33000 Bordeaux, France

Abstract

Catheter-based cardiac ablation, such as radiofrequency ablation (RFA) and pulsed electric field ablation (PFA), is the treatment of choice for atrial fibrillation (AF). However, the underlying phenomena and differences between RFA and PFA are not well understood. In this paper, we propose mathematical modeling of the cardiac electric signal of a cardiac domain containing an ablated area by RFA or PFA. Both types of ablation consist of the isolation of the pulmonary vein, but we describe them differently by using appropriate transmission conditions. More specifically, we assume that in the case of RFA, both intracellular and extracellular potentials are affected, leading to Kedem-Katchalsky type conditions at the interface. In contrast, in the case of PFA, we assume an isolation of the intracellular potential (due to the cardiomyocytes death induced by electroporation) whereas the extracellular potential is continuous. Numerical simulations in a context of AF show that PFA and RFA lead to isolation of the pulmonary vein. Our modeling also enables to propose a numerical explanation for the higher rate of fibrillation recurrence after RFA compared with PFA.

Keywords: Electrocardiology modeling; Radiofrequency ablation; Pulsed electric field ablation.

1 Introduction

Cardiac arrhythmias are irregularities in the heartbeat that result in chaotic electrical waves. While most of cardiac arrhythmias are benign, some of them can directly affect the pumping function of the heart, leading then to stroke or heart failure. Isolation of the pulmonary veins by catheter ablation has become the treatment of choice for atrial fibrillation (AF). The goal is to isolate the pulmonary veins from which the fibrillation is supposed to originate by physical procedures such as thermal ablation (cryoablation [17] or radiofrequency ablation (RFA) [10]), and more recently pulsed electric field ablation (PFA), which is based on nonthermal irreversible electroporation.

Despite the great interest that RFA and PFA have generated in the treatment of AF, there is still a lack of understanding – and thus modelling – of the underlying biophysical phenomena of these different therapies. On one hand, it is well known that RFA ablation leads to coagulation necrosis with complete loss of cellular and vascular architecture [2] by leaving a scar composed of a fibrotic tissue. On the other hand, PFA is known to destroy mainly the cardiomyocytes, but the tissue scaffold is preserved [12, 3]. Therefore,

the physical properties of the cardiac tissue after RFA and PFA are very different, although they have the same goal, which is to isolate the pulmonary vein.

Recent medical studies have shown that the recurrence of atrial fibrillation with PFA [15] is on the order of 15%, compared with 30% with RFA [19]. We hypothesize that these treatment failures can somehow be explained by the long-lasting changes in the electrical properties of the tissue after ablation.

Well-designed mathematical modeling could help to better understand the effects of PFA on cardiac electrical wave and to develop numerical criteria for treatment evaluation. For example, one of the challenges is to derive electroporation models at the cellular or tissue level. This is a very interesting question, but in this work we focus on another one. More precisely, we propose a mathematical modeling of the cardiac electrical signal of a cardiac domain containing an area ablated by RFA or PFA. We study the effects of this treated area on the propagation of the electrical wave, known to correspond to the so-called bidomain model [18] in cardiac domain, through well-adapted transmission conditions across the treated region.

After a detailed presentation of the mathematical modeling in Section 2, we perform numerical simulations in a realistic configuration in Section 3. We show that our models are able to represent very well the isolation of a pulmonary vein by RFA and PFA ablation, and we propose an explanation for the higher recurrence rate of fibrillation after RFA.

2 Modeling

2.1 Geometrical setting

For numerical purposes, it is convenient to consider the cardiac tissue as a midsurface as suggested in [4], to avoid meshing the thin volume. This configuration has been found to be particularly well suited for the very thin wall of the atria.

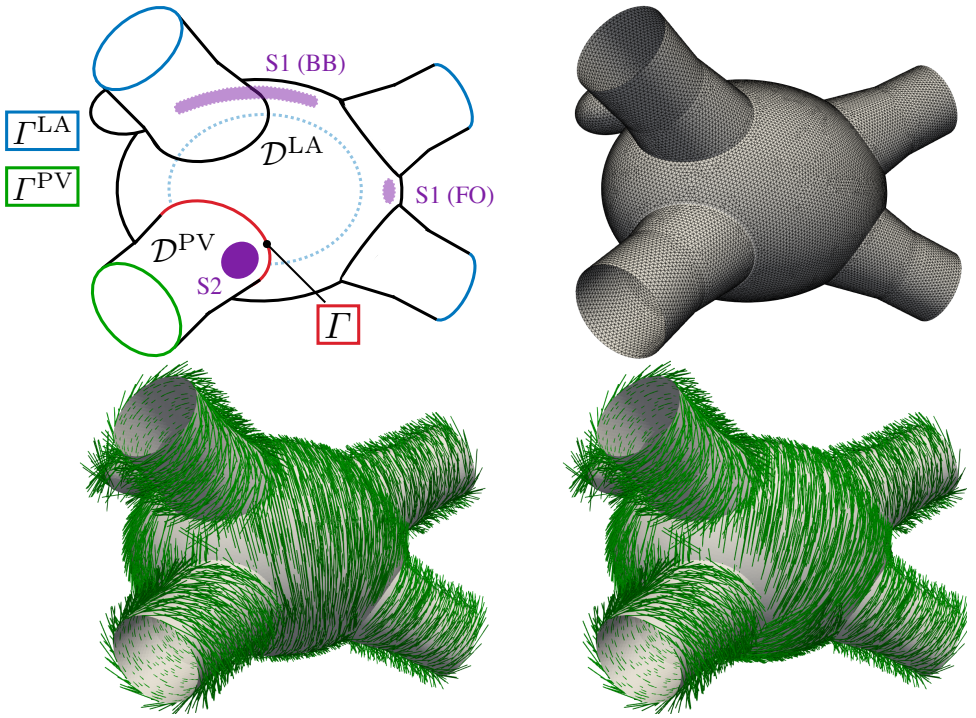

Figure 1: Geometrical setting. Domains with interfaces (left-top), computational mesh (right-top), fibers orientation at the endocardium (left-bottom) and at the epicardium (right-bottom).

2.1.1 Domains of interest and mesh

The geometric configuration is presented in Fig. 1. The left atrium, denoted by $\mathcal{D}^{\mathrm{LA}}$ is a 2D surface separated from one of the 4 pulmonary veins denoted by $\mathcal{D}^{\mathrm{PV}}$ by the interface Γ. For the sake of simplicity, we only focus on the isolation of one pulmonary vein even though in clinical cardiac ablation the 4 veins are isolated. We denote by Γ^{PV} the outer boundary of $\mathcal{D}^{\mathrm{PV}}$, while the 3 other outer boundaries of the pulmonary veins are denoted by Γ^{LA} (see Fig. 1). The whole domain of interest is denoted by $\mathcal{D}$:

$$\mathcal{D} = \mathcal{D}^{\mathrm{LA}} \cup \Gamma \cup \mathcal{D}^{\mathrm{PV}}.$$

2.1.2 Fibers orientation

It is well-known that the fibers orientation impacts the propagation of the electrical wave on the heart. Chapelle *et* al. have proposed an efficient model of the electrical properties of the fibers [4] allowing to consider fiber variations inside the thickness of the atria. They introduce the following tensors: $\bar{\bar{I}}$ denotes the identity tensor in the tangential plane, $\bar{\tau}_0$ denotes a unit vector, linked to the fiber direction of the midsurface of the atria, and $\bar{\tau}_0^{\perp}$ is such that $(\bar{\tau}_0, \bar{\tau}_0^{\perp})$ gives an orthonormal basis to the tangent plane. Eventually, they introduce the functions $I_0(\theta) = \frac{1}{2} + \frac{1}{4\theta}\sin(2\theta)$ and $J_0(\theta) = 1 - I_0(\theta)$ to describe the effect of a variation of a 2θ angle of the direction of the fibers across the wall. Then, the intra- and extra-cellular conductivity tensors denoted by $\bar{\bar{\sigma}}_i$ and $\bar{\bar{\sigma}}_e$ respectively are defined by

$$\bar{\bar{\sigma}}_{i,e} = \sigma_{i,e}^t \bar{\bar{I}} + (\sigma_{i,e}^t - \sigma_{i,e}^l)\left[I_0(\theta)\bar{\tau}_0 \otimes \bar{\tau}_0 + J_0(\theta)\bar{\tau}_0^{\perp} \otimes \bar{\tau}_0^{\perp}\right], \qquad \text{in } \mathcal{D}. \tag{1}$$

where $\sigma_{i,e}^t$ and $\sigma_{i,e}^l$ denote the conductivity coefficients in the intracellular medium measured along and across the fiber direction, respectively.

2.2 Surface bidomain model in the atrium

To model the electrical wave propagation, we consider the well-known bidomain model [18], widely studied in literature. It consists of a non linear degenerate parabolic partial differential equation (PDE), coupled with an ordinary differential equation (ODE), representing the activity of the ion channels. In particular, considering a quite simple phenomenological ionic model, equations can be rewritten in terms of the intracellular potential u_i, the extracellular potential u_e and the ionic variable w. The system of equations writes, for any $t > 0$,

$$A_m(C_m\partial_t v_m + I_{ion}(v_m, w)) - \nabla \cdot (\bar{\bar{\sigma}}_i \cdot \nabla u_i) = 0, \qquad \mathcal{D}, \tag{2a}$$

$$\nabla \cdot (\bar{\bar{\sigma}}_e \cdot \nabla u_e) + \nabla \cdot (\bar{\bar{\sigma}}_i \cdot \nabla u_i) = 0, \qquad \mathcal{D}, \tag{2b}$$

$$\partial_t w + g(v_m, w) = 0, \qquad \mathcal{D}, \tag{2c}$$

$$v_m = u_i - u_e, \qquad \mathcal{D}, \tag{2d}$$

where the functions I_{ion} and g are defined as in the model proposed by Mitchell and Schaeffer [14], A_m, the fraction of membrane area per unit volume and C_m, the membrane capacitance per unit surface. We assume that the heart is isolated, so we make the standard assumption that the extra- and intra-cellular currents do not propagate outside the heart meaning that we consider Neumann homogeneous boundary conditions on $\partial\mathcal{D}$, for any time $t > 0$,

$$(\bar{\bar{\sigma}}_i \cdot \nabla u_i) \cdot \bar{n} = 0, \quad (\bar{\bar{\sigma}}_e \cdot \nabla u_e) \cdot \bar{n} = 0, \qquad \text{on } \partial\mathcal{D}, \tag{2e}$$

$\bar{n}$ being the normal vector to $\partial\mathcal{D}$ outwardly directed from $\mathcal{D}$ towards the exterior.

2.3 Transmission conditions through Γ

The above system (2) has to be complemented with initial conditions for u_i, u_e and w at time $t = 0$ and a Gauge condition on u_e to fix the constant. In this paper, we impose

$\int_{\mathcal{D}} u_e \, dx = 0$. More importantly, to close the system, appropriate transmission conditions through the interface Γ must be prescribed. They depend on the ablation that we consider and they are presented in the following subsections. We first introduce few notations. Denote by Γ^+ (resp. Γ^-) the interfaces

$$\Gamma^+ = \Gamma \cap \overline{\mathcal{D}^{\mathrm{PV}}}, \quad \Gamma^- = \Gamma \cap \overline{\mathcal{D}^{\mathrm{LA}}},$$

where $\overline{\mathcal{D}^{\mathrm{LA}}}$ denotes the adherence of $\mathcal{D}^{\mathrm{LA}}$, *mutatis mutandis* for $\overline{\mathcal{D}^{\mathrm{PV}}}$. For any function u defined on $\mathcal{D}$ and discontinuous through Γ, the jump of u across Γ is

$$[\![u]\!]_{|\Gamma} = u_{|\Gamma^+} - u_{|\Gamma^-}.$$

2.3.1 Radiofrequency Ablation

To model the effect of RFA, we consider the well-known Kedem–Katchalsky transmission conditions – initially introduced in [11] – which read

$$\alpha [\![u_e]\!]_{|\Gamma} = \left((\bar{\bar{\sigma}}_e \cdot \nabla u_e) \cdot \bar{n}\right)_{|\Gamma^+} = \left((\bar{\bar{\sigma}}_e \cdot \nabla u_e) \cdot \bar{n}\right)_{|\Gamma^-}, \tag{3a}$$

$$\alpha [\![u_i]\!]_{|\Gamma} = \left((\bar{\bar{\sigma}}_i \cdot \nabla u_i) \cdot \bar{n}\right)_{|\Gamma^+} = \left((\bar{\bar{\sigma}}_i \cdot \nabla u_i) \cdot \bar{n}\right)_{|\Gamma^-}, \tag{3b}$$

here $\bar{n}$ is the normal vector to Γ oriented from Γ^- towards Γ^+. The coefficient α is a positive constant homogeneous to a surface conductance. It takes into account the fact that the treated region has a higher resistance due to RFA than the healthy tissue. This parameter α is crucial because it is responsible for whether or not the transmembrane potential wave can overcome the Γ interface. In particular, when $\alpha = 0$, it is equivalent to a complete decoupling of the two domains $\mathcal{D}^{\mathrm{LA}}$ and $\mathcal{D}^{\mathrm{PV}}$, resulting in a perfect isolation of the pulmonary vein.

In the asymptotic regime $\alpha \gg 1$, the potentials u_e and u_i become asymptotically continuous. The Kedem-Katchalsky can then be seen as a penalty term which weakly enforces the continuity of the potential through the interface Γ [1]. In the following numerical section, we consider different values of α showing different levels of pulmonary vein isolation.

2.4 Pulsed Field Ablation

It has been experimentally observed that PFA preserves the tissue scaffold and targets the myocardium through the nonthermal, irreversible electroporation process. After PFA, the mechanical properties (stiffness, elasticity...) of the cardiac tissue are preserved, whereas the electrical functionalities of the ablation area are altered [2]. Most likely, PFA leads to local death of cardiomyocytes, which are then replaced by nonexcitable fibroblasts.

Based on these considerations, we propose to model the electrical effect of PFA by a continuity of both the extracellular potential u_e and the extracellular normal flux $(\bar{\bar{\sigma}}_e \cdot \nabla u_e) \cdot \bar{n}$, while assuming that the intracellular potential of $\mathcal{D}^{\mathrm{LA}}$ is isolated from the intracellular potential of $\mathcal{D}^{\mathrm{PV}}$, thus using a homogeneous Neumann boundary condition for u_i. In other words the transmission conditions describing the effect of PFA read

$$[\![u_e]\!]_{|\Gamma} = 0, \ [\![(\bar{\bar{\sigma}}_e \cdot \nabla u_e) \cdot \bar{n}]\!]_{|\Gamma} = 0, \tag{4a}$$

$$\left((\bar{\bar{\sigma}}_i \cdot \nabla u_i) \cdot \bar{n}\right)_{|\Gamma^+} = \left((\bar{\bar{\sigma}}_i \cdot \nabla u_i) \cdot \bar{n}\right)_{|\Gamma^-} = 0. \tag{4b}$$

The mathematical justification of these conditions is beyond the scope of the present paper and will be presented in a forthcoming mathematical paper. Roughly speaking, these conditions arise from an asymptotic analysis in which the small parameter is the thickness of the electroporated region and its low intracellular conductivity tensor.

3 Numerical illustrations

The aim of this section is to compare the transmembrane potential v_m and the extracellular potential u_e satisfying (2) with either the transmission conditions for RFA (3) or the transmission conditions for PFA (4). For the sake of simplicity, we assume that the treated region behaves identically along the interface Γ. It means that the parameter α in (3) is assumed to be constant.

3.1 Mesh, fibers and numerical schemes

The simplified geometry of the left atrium is constructed as an ellipsoid 50mm long and 35mm high (see Fig. 1). Its depth is intersected by a plane corresponding to the position of the mitral valve. Four pulmonary veins – modeled by cutting cones with a mean diameter of 13mm – are added. The appendage is modeled by an ellipsoid of 10mm $\times$ 5mm $\times$ 5mm. The mesh, presented in Fig. 1 has been generated by `Gmsh` [6]. The surface mesh is composed of 26141 nodes and 51904 triangular elements. The fibers directions – needed to build the tensors (1) – at the endocardium and epicardium are derived according to the literature [8, 13].

The numerical illustrations have been obtained using `FreeFem++` [7], a PDE solver based on finite element method. All the problems are solved with a BDF2 semi-implicit scheme ($\Delta t = 0.01$ms) to deal with the nonlinear term I_{ion} and with P1 elements. To numerically solve the transmission conditions of RFA with fibrosis, we consider a weak coupling. Indeed, the condition leads to a Neumann condition in which we use the trace of the solution on Γ^- (resp. Γ^+) at the previous time step when solving the solution in PV domain (resp. LA domain). To numerically solve the transmission conditions of PFA, we use a Schwarz-type algorithm in which the penalty parameter is fixed at 2. This value has been chosen very carefully through a mathematical study, following [9]. Mesh, fibers and codes are available here: https://gitlab.inria.fr/snatipol/af-pfa-rfa.

3.2 Numerical illustrations before ablation

To compare the effects of the two ablations considered, a simulation corresponding to atrial fibrillation before ablation is proposed.

Physiologically, the depolarization wave that triggers the heartbeat is initiated in the sinoatrial node in the right atrium. It then propagates to the left atrium via two electric pathways: the fastest leading to Bachmann's bundles (BB) and the second to the fossa ovalis (FO). The BB are modeled as two ellipsoids located at the top of the atrium near the appendage. The FO is located on the right side of the left atrium, on the wall between the right and left atria. They are also shown in Figure 1. The depolarization wave reaches the FO at $t = 10$ms after depolarization of the BB corresponding to $t = 0$ms. To generate the AF synthetically, we use a standard S1-S2 protocol [5]. The S1 stimulus corresponds to the BB and the FO stimulus. The S2 stimulus location is near the left pulmonary inferior vein, see Figure 1. Pulmonary veins are known to be prone to frequent reentry. The S2 stimulus is triggered at $t = 356$ ms. Parameters were set in [16].

The first column of Figure 2 shows time snapshots of the transmembrane potential before ablation. One first sees the healthy depolarization occurring during the first 90ms – see 20, 44, and 70ms snapshots – followed by the healthy repolarization – see 200ms snapshot – and by the second stimulus illustrating a pathological area of one of the pulmonary veins – see 356ms snapshot – that triggers a pathological wave that unfolds in the left atrium – see 430 and 500ms snapshots.

3.3 Effects on the electric signal

The second column of Figure 2 gives the transmembrane potential corresponding to successful RFA (Equation (3), $\alpha = 10^{-4}$). Because the two regions are nearly decoupled, the pulmonary vein is well isolated: there is no entry of the wave into the left atrium, see

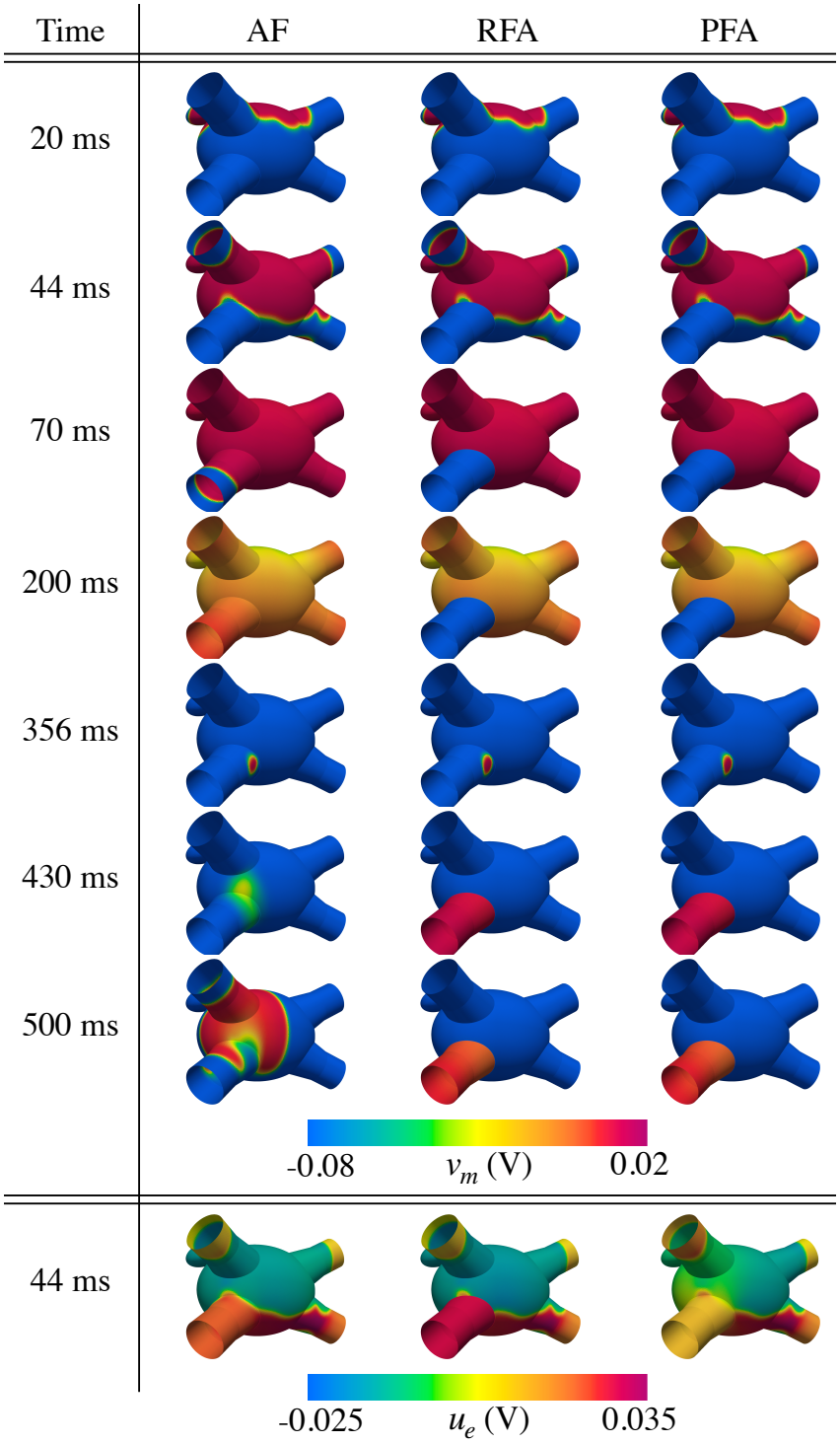

Figure 2: First column: before ablation. Second column: successful RFA (Equation (3), $\alpha = 10^{-4}$). Third column: successful PFA. Lines 1 to 7: Snapshots of transmembrane potential v_m. Last line: Snapshot of extracellular potential u_e.

356, 430, and 500ms snapshots. Uncoupling is also seen in the evolution of the extracellular potential, shown in the last line of the same figure at time 44ms. The third column of Figure 2 corresponds to a successful PFA. One can first see that there is no entry of the transmembrane wave, showing the success of the ablation. However and contrary to RFA

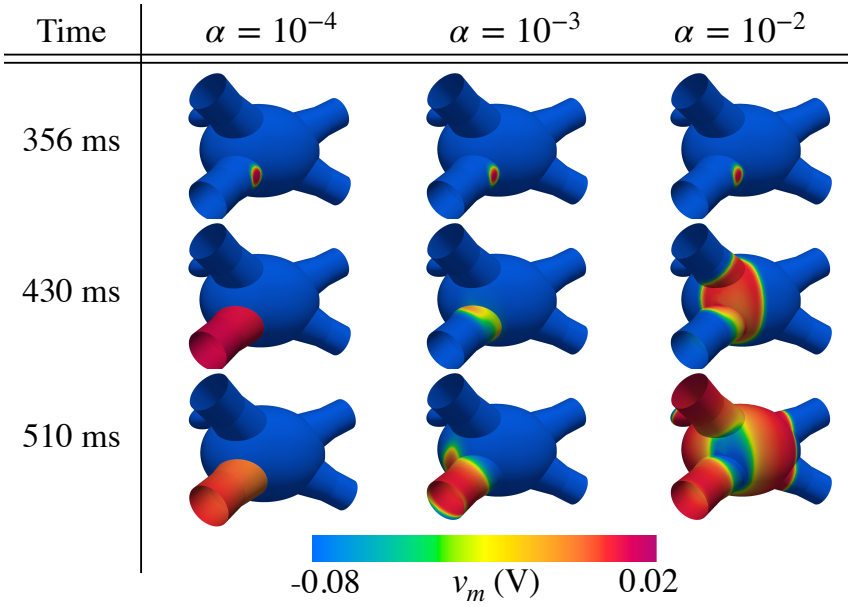

Figure 3: Snapshots of transmembrane potential v_m in 3 situations of RFA corresponding to transmission conditions (3). First column: $\alpha = 10^{-4}$. Second column: $\alpha = 10^{-3}$. Third column: $\alpha = 10^{-2}$.

(second column), the PFA maintains the continuity of the extracellular potential u_e, see the last line of Figure 2.

The effects of the α parameter are shown in Figure 3. One can see that as it increases – see the second and the third columns ($\alpha = 10^{-3}$ and $\alpha = 10^{-2}$) – the wave crosses the interface from the pulmonary vein to the left atrium, resulting in a restart of the atrial fibrillation even though the propagation of the wave is delayed. The larger the value of α, the smaller the delay here. The increase in α can be viewed as the emergence of electrical pathways between $\mathcal{D}^{\mathrm{LA}}$ and $\mathcal{D}^{\mathrm{PV}}$.

4 Conclusion

In this work, we propose a mathematical modeling of the cardiac electric signal of a cardiac domain containing a region ablated by RFA or PFA. It consists in determining the transmission conditions of the very classical bidomain model at the interface of the ablated area. Our goal was to propose a mathematical explanation for the lower recurrence of AF after PFA compared with RFA as reported in the literature [15, 19]. Thanks to well-designed transmission conditions, we were able to model the complete or partial disconnection – for both transmembrane and extracellular potentials – of the pulmonary vein. Partial disconnection can be seen as the emergence of electrical pathways between the atrium and the pulmonary vein. It could be caused by the development of necrotic fibrosis after RFA, which is not the case in PFA. Thus, our work suggests that both RFA and PFA lead to isolation of the pulmonary veins with respect to the electrical signal, but the nature of these isolations is very different. We hypothesize that RFA-induced fibrosis may lead to conduction pathways. This work is a first step towards a fine modeling of the effects of a tissue region ablated by PFA in cardiology.

5 Acknowledgement

The authors gratefully acknowledge support from the French Agence Nationale de la Recherche (ANR) (grant ANR-22-CE45-0014-01, project MIRE4VTach), from the Atrial

Fibrillation Chair of the IHU Liryc, from the Fondation Bordeaux Université, from the Fondation Lefoulon-Delalande, and from the French Federation of Cardiology - Grands projets - 2022 (project DIELECTRIC).

References

[1] I. Babuška. The finite element method with penalty. Mathematics of computation, 27(122):221–228, 1973.

[2] B. E. Bulvik, N. Rozenblum, S. Gourevich, M. Ahmed, A. V. Andriyanov, E. Galun, and S. N. Goldberg. Irreversible electroporation versus radiofrequency ablation: a comparison of local and systemic effects in a small-animal model. Radiology, 280(2):413–424, 2016.

[3] G. Caluori, E. Odehnalova, T. Jadczyk, M. Pesl, I. Pavlova, L. Valikova, S. Holzinger, V. Novotna, V. Rotrekl, A. Hampl, et al. AC pulsed field ablation is feasible and safe in atrial and ventricular settings: a proof-of-concept chronic animal study. Frontiers in bioengineering and biotechnology, 8:552357, 2020.

[4] D. Chapelle, A. Collin, and J.-F. Gerbeau. A surface-based electrophysiology model relying on asymptotic analysis and motivated by cardiac atria modeling. Mathematical Models and Methods in Applied Sciences, 23(14):2749–2776, 2013.

[5] P. C. Franzone, L. F. Pavarino, and S. Scacchi. Mathematical cardiac electrophysiology, volume 13. Springer, 2014.

[6] C. Geuzaine and J.-F. Remacle. Gmsh: A 3-D finite element mesh generator with built-in pre-and post-processing facilities. International journal for numerical methods in engineering, 79(11):1309–1331, 2009.

[7] F. Hecht, O. Pironneau, A. Le Hyaric, and K. Ohtsuka. Freefem++ manual, 2005.

[8] S. Y. Ho, R. H. Anderson, and D. Sánchez-Quintana. Atrial structure and fibres: morphologic bases of atrial conduction. Cardiovascular research, 54(2):325–336, 2002.

[9] F. B.-F. Hubert. Méthodes de décomposition de domaine de type schwarz. 2014.

[10] J. Joseph and K. Rajappan. Radiofrequency ablation of cardiac arrhythmias: past, present and future. QJM: An International Journal of Medicine, 105(4):303–314, 2012.

[11] O. Kedem and A. Katchalsky. A physical interpretation of the phenomenological coefficients of membrane permeability. The Journal of general physiology, 45(1):143–179, 1961.

[12] J. Koruth, K. Kuroki, J. Iwasawa, Y. Enomoto, R. Viswanathan, R. Brose, E. D. Buck, M. Speltz, S. R. Dukkipati, and V. Y. Reddy. Preclinical evaluation of pulsed field ablation: electrophysiological and histological assessment of thoracic vein isolation. Circulation: Arrhythmia and Electrophysiology, 12(12):e007781, 2019.

[13] M. W. Krueger, V. Schmidt, C. Tobón, F. M. Weber, C. Lorenz, D. U. Keller, H. Barschdorf, M. Burdumy, P. Neher, G. Plank, et al. Modeling atrial fiber orientation in patient-specific geometries: a semi-automatic rule-based approach. In Functional Imaging and Modeling of the Heart: 6th International Conference, FIMH 2011, New York City, NY, USA, May 25-27, 2011. Proceedings 6, pages 223–232. Springer, 2011.

[14] C. C. Mitchell and D. G. Schaeffer. A two-current model for the dynamics of cardiac membrane. Bulletin of mathematical biology, 65(5):767–793, 2003.

[15] V. Y. Reddy, S. R. Dukkipati, P. Neuzil, A. Anic, J. Petru, M. Funasako, H. Cochet, K. Minami, T. Breskovic, I. Sikiric, et al. Pulsed field ablation of paroxysmal atrial fibrillation: 1-year outcomes of IMPULSE, PEFCAT, and PEFCAT II. Clinical Electrophysiology, 7(5):614–627, 2021.

[16] E. Schenone, A. Collin, and J.-F. Gerbeau. Numerical simulation of electrocardiograms for full cardiac cycles in healthy and pathological conditions. International journal for numerical methods in biomedical engineering, 32(5):e02744, 2016.

[17] A. C. Skanes, G. Klein, A. Krahn, and R. Yee. Cryoablation: potentials and pitfalls. Journal of cardiovascular electrophysiology, 15:S28–S34, 2004.

[18] L. Tung. A bi-domain model for describing ischemic myocardial dc potentials. PhD thesis, Massachusetts Institute of Technology, 1978.

[19] F. H. Wittkampf and H. Nakagawa. RF catheter ablation: lessons on lesions. Pacing and Clinical Electrophysiology, 29(11):1285–1297, 2006.